LASER & PHOTONICS REVIEWS

www.lpr-journal.org

Hydrothermal Synthesis of Yb^{3+}: $LuLiF_4$ Microcrystals and Laser Refrigeration of Yb^{3+}: $LuLiF_4$/Silicon-Nitride Composite Nanostructures

*Elena A. Dobretsova, Xiaojing Xia, Anupum Pant, Matthew B. Lim, Michael C. De Siena, Kirill N. Boldyrev, Anastasia D. Molchanova, Nadezhda N. Novikova, Sergei A. Klimin, Marina N. Popova, Yueyang Chen, Arka Majumdar, Daniel R. Gamelin, and Peter J. Pauzauskie**

The hydrothermal synthesis and characterization of 10%Yb^{3+}:$LiLuF_4$ (LLF) microcrystals are reported. A combination of X-ray diffraction (XRD) analysis, analytical transmission electron microscopy (TEM), scanning TEM (STEM), energy-dispersive X-ray (EDX) spectroscopy), temperature-dependent Fourier-transform infrared (FTIR) spectroscopy, and photoluminescence (PL) measurements confirm a scheelite ($I4_1/a$) phase and substitutional doping of Yb^{3+} within the microcrystals. Laser cooling to more than 20 K below room temperature in vacuum (10^{-3} torr) is demonstrated when irradiating individual microcrystals using a near-infrared pumping wavelength (λ = 1020nm) at a laser power of 40 mW (irradiance of 0.85 MW cm^{-2}). The use of these microcrystals is further demonstrated for solid-state laser refrigeration of an electron-transparent silicon-nitride (Si_3N_4) TEM window. A combination of internal luminescence thermometry, heat-transfer modeling, and control measurements on lithographically patterned Si_3N_4 optical cavities is used to demonstrate successful bulk laser cooling of Si_3N_4 TEM windows by ≈15 K below room temperature, opening new opportunities for contactless in situ TEM refrigeration.

1. Introduction

Recent advances with in situ[1–18] and cryo-TEM imaging[19–29] have enabled a wide range of new experimental capabilities for materials characterization. Conventional methods to refrigerate samples during in situ TEM measurements involve continuous evaporation of liquid nitrogen. The liquid nitrogen must be replenished to maintain long-term operation of the microscope, and may degrade the quality of high-resolution images due to mechanical jitter from evaporating nitrogen bubbles. Solid-state laser refrigeration offers a promising alternative approach to in situ refrigeration of TEM samples. The development of bulk Czochralski single crystals of Yb^{3+}:$YLiF_4$ with record-high purity[30–32] has enabled the first demonstration of solid-state laser refrigeration to cryogenic

Dr. E. A. Dobretsova, Dr. A. Pant, Dr. M. B. Lim, Prof. P. J. Pauzauskie
Department of Materials Science & Engineering
University of Washington
Seattle, WA 98195, USA
E-mail: peterpz@uw.edu

Dr. E. A. Dobretsova
Prokhorov General Physics Institute of the Russian Academy of Sciences
Moscow 119991, Russia

X. Xia
Molecular Engineering and Science Institute
University of Washington
Seattle, WA 98195, USA

Dr. M. C. De Siena, Prof. D. R. Gamelin
Department of Chemistry
University of Washington
Seattle, WA 98195, USA

Dr. K. N. Boldyrev, Dr. A. D. Molchanova, Prof. M. N. Popova
Laboratory of Fourier Spectroscopy
Institute of Spectroscopy of the Russian Academy of Sciences
Moscow 108840, Russia

Dr. N. N. Novikova, Dr. S. A. Klimin
Laboratory of Condensed Matter Spectroscopy
Institute of Spectroscopy of the Russian Academy of Sciences
Moscow 108840, Russia

Dr. Y. Chen, Prof. A. Majumdar
Department of Electrical and Computer Engineering
University of Washington
Seattle, WA 98195, USA

Prof. A. Majumdar
Department of Physics
University of Washington
Seattle, WA 98195, USA

Prof. P. J. Pauzauskie
Physical & Computational Science Directorate
Pacific Northwest National Laboratory
Richland, WA 99352, USA

The ORCID identification number(s) for the author(s) of this article can be found under https://doi.org/10.1002/lpor.202100019

DOI: 10.1002/lpor.202100019

temperatures using continuous-wave near-infrared laser excitation with no moving parts or mechanical jitter. More recently, the laser refrigeration of water and physiological electrolytes has been demonstrated using 10%Yb^{3+}:$YLiF_4$[33] and 10%Yb^{3+}:$NaYF_4$[34] microcrystals synthesized via a scalable, low-cost hydrothermal process. The absence of moving parts or mechanical jitter makes laser refrigeration particularly attractive for in situ refrigeration in TEM experiments. In this work we demonstrate that Yb^{3+}:$LuLiF_4$ microcrystals synthesized hydrothermally can be used to optically refrigerate electron-transparent Si_3N_4 windows frequently used for in situ TEM imaging. These results open new possibilities for in situ cooling and cryo-TEM.

In 1929, Pringsheim predicted that sodium vapor could be optically refrigerated through the absorption of a photon followed by the emission of a blue-shifted (anti-Stokes) photon.[35] Solid-state laser refrigeration relies on a similar process where a low-energy photon is absorbed by the solid to create an electronic excited state with a lifetime long enough to absorb heat from the surrounding material. Following thermal upconversion, the excited state relaxes by emitting a blue-shifted photon with an energy determined by the energy of the original excitation photon ($h\nu$) plus the energy of absorbed optical phonons. The emission of the upconverted photon cools the solid by transporting both the excitation photon and the absorbed phonons from the solid.[36]

Due to their extremely high PL quantum efficiencies, rare-earth (RE) doped solids were suggested in 1961 for use in laser cooling.[37] In 1968, Kushida and Geusic observed reduction of heating by subjecting single crystals of Nd-doped yttrium aluminum garnet (Nd^{3+}:YAG) to intense 1064 nm laser radiation.[38] Epstein and coworkers reported the first experimental net cooling of a solid ZBLAN:Yb^{3+} glass sample by 0.3 K following NIR laser excitation.[39] More recently a temperature drop of 8.8 K was observed in a Yb^{3+}:YAG crystal in air.[40]

Fluoride single crystals exhibit properties promoting laser cooling and distinguishing them from other RE-hosts, including weak thermal lensing, high transparency in a wide wavelength range from the UV to the IR, a low index of refraction, and low phonon energies suppressing nonradiative relaxation between adjacent energy levels. In comparison with amorphous glass host materials, crystalline host materials, as a rule, demonstrate reduced inhomogeneous broadening and larger optical absorption coefficients. Among potential RE host lattices, Yb^{3+}:$YLiF_4$ (YLF) single crystals have demonstrated the lowest laser cooling temperatures reported to date. YLF has been developed over the last 60 years as a host for rare-earth ions.[41–49] In 2010, Sheik-Bahae's group showed that a 5%Yb^{3+}:YLF bulk crystal can be optically cooled to cryogenic temperatures (≈155 K) without the use of cryogens or mechanical refrigeration.[30] This result was attained by making use of the well-defined Stark manifold of Yb^{3+} electronic levels within the crystalline RE-host. Further thermal management and enhanced absorption led to a demonstration of laser cooling to 119 K, reaching NIST's designated range of cryogenic temperatures (<123 K) for the first time.[31] The lowest reported temperature for solid-state laser refrigeration (91 K) was achieved using single crystals of 10%Yb^{3+}:YLF by tuning the excitation of the crystal to the Yb^{3+} E_4-E_5 resonance at 1020 nm in a Herriot cell.[32] More recently an optically-trapped 10%Yb^{3+}:YLF nanocrystal was reported to cool to 130 K in vacuum.[50]

One challenge for growing $YLiF_4$ is that the material melts incongruently, which causes complications during bulk Czochralski crystal growth. This issue has motivated the search for crystalline host materials for Yb^{3+} that melt congruently, such as $LuLiF_4$ (LLF). $LuLiF_4$ is even better suited for laser cooling than $YLiF_4$ because the lowest peak in its phonon density of states is situated at a lower energy (58 cm^{-1} vs 73 cm^{-1} for $YLiF_4$).[51] Laser cooling of Yb^{3+}-doped $LuLiF_4$ (Yb^{3+}:LLF) bulk single crystals synthesized by the Czochralski method has been pursued since 2014.[52–56] A drop of 11 K from room temperature was reported for a 5%Yb^{3+}:LLF crystal in air pumped by a 3 W CW fiber laser (λ = 1020 nm), as observed by a thermal camera.[53] The cooling power and efficiency were estimated to be ≈14.5 mW and ≈1.9%, respectively. Recently, laser cooling of a 5%Yb^{3+}:LLF crystal placed in a vacuum chamber with an ambient temperature of ≈294.5 K has achieved a temperature below the limit of current thermoelectric coolers (≈180 K).[55]

One challenge in the field of solid-state laser refrigeration is that growing single crystals using the Czochralski process requires the use of high temperatures (>500 °C) with hydrofluoric acid (HF). High temperatures increase the concentration of crystallographic point defects in the material, and HF carries significant safety hazards. Recently, it has been demonstrated that low-cost, low-temperature, hydrothermal processing can be used to grow both $YLiF_4$ and $NaYF_4$ materials that are capable of solid-state laser refrigeration. However, laser refrigeration of hydrothermally grown LLF has not been reported to date. In this work, we report the hydrothermal synthesis of Yb^{3+}-doped LLF microcrystals and demonstrate their application in the laser refrigeration of electron-transparent TEM windows and optical microcavities.

2. Results and Discussion

Figure 1a summarizes the hydrothermal synthesis of 10%Yb^{3+}:LLF microcrystals (see Experimental section for details). X-ray diffraction (XRD) analysis shows a scheelite structure (ICDD PDF number: 04-002-3255) with space group $I4_1/a$ (Figure 1b; Figure S1, Supporting Information). Scanning electron microscopy (SEM) shows that the Yb^{3+}:LLF crystals have a truncated tetragonal bipyramidal morphology and size distribution range from 500 nm to 20 μm (Figure 1c). Energy-dispersive X-ray spectroscopy (EDS) composition analysis on an individual 10%Yb^{3+}:LLF microcrystal taken on the SEM points to the presence of Lu, Yb, and F (Figure S2, Supporting Information). TEM data taken from milled particles of 10%Yb^{3+}:LLF confirm this result (Figure S3, Supporting Information). Temperature-dependent FTIR transmission measurements reveal the phonon spectra of lithium-lutetium double fluoride in the range of 100–500 cm^{-1} (Figure 1d). Eight modes, four A_u and four E_u modes, are infrared-active. The interpretation of spectral modes has been reported previously on the basis of polarized infrared-reflection measurements on $LiLnF_4$ (Ln = Y, Yb, Tm, Er, Ho) single crystals, using a factor-group analysis approach.[46,57] Spectral bands change little with decreasing temperature. The room-temperature attenuated total reflectance (ATR) FTIR spectrum includes weak bands in the region of 1000–4000 cm^{-1} corresponding to atmospheric water and carbon dioxide. (Figure S4, Supporting Information).

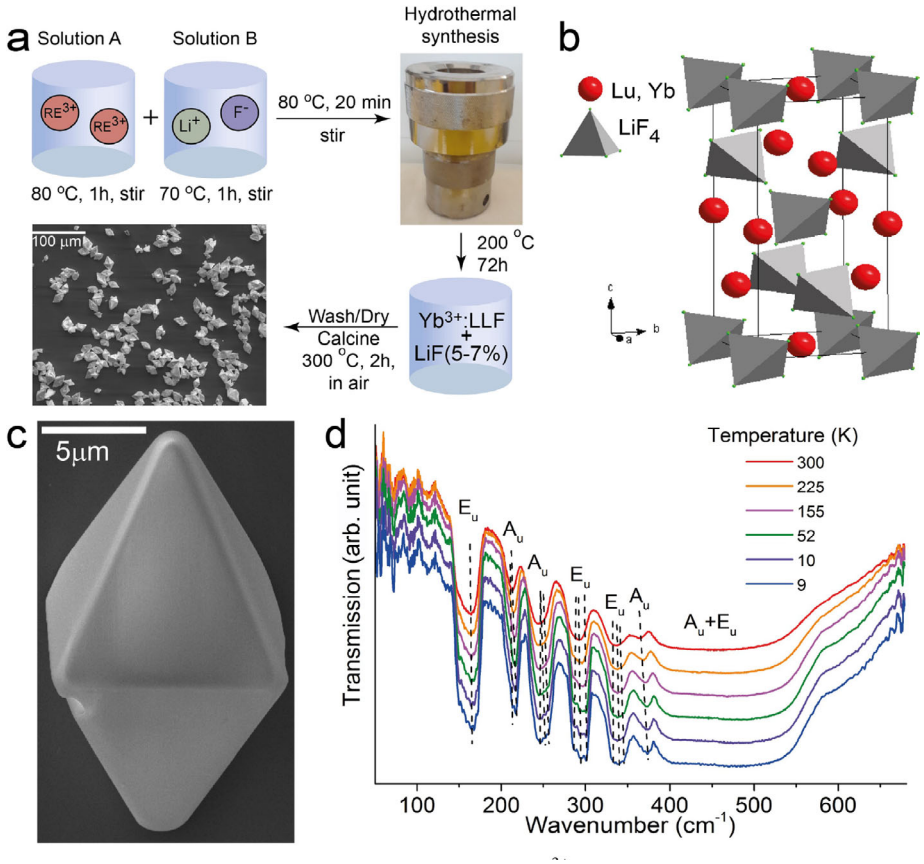

Figure 1. Synthesis and characterization of 10%Yb^{3+}:LLF microcrystals. a) Schematic of hydrothermal synthesis of 10%Yb^{3+}:LLF microcrystals; b) Schematic of a Scheelite crystal structure of 10%Yb^{3+}:LLF with $I4_1/a$ space group symmetry; c) Scanning electron microscope image of a faceted 10%Yb^{3+}:LLF particle exhibiting truncated tetragonal bipyramidal morphology. Scale bar = 5 µm. d) Temperature-dependent FTIR transmission spectrum of 10%Yb^{3+}: LLF between 9 and 300 K.

To collect PL spectra of hydrothermal Yb^{3+}:LLF microcrystals, individual grains were transferred to an optical fiber for thermal isolation and optically excited using pulsed (5 ms) laser excitation with wavelength $\lambda = 1020$ nm. A schematic of the sample's thermal isolation is shown in **Figure 2**a and an optical micrograph of suspended 10%Yb^{3+}:LLF grains is shown in Figure 2b. In Yb^{3+}:LLF, the Yb^{3+} $^2F_{7/2}$ and $^2F_{5/2}$ multiplets split into 4 and 3 levels, respectively, as illustrated in Figure 2c. The PL excitation wavelength was chosen to pump the lowest crystal-field transition of Yb^{3+}, exciting the ion from the E_4 to the E_5 level. A representative Yb^{3+} spectrum in the range 900–1050 nm is shown in Figure 2c and Figure S5 (Supporting Information). The Yb^{3+} PL lifetime was measured to be 1.9 ms at room temperature (Figure S6, Supporting Information). PL spectra were taken at low temperature (77 K) and room temperature allowing for the specific assignment of crystal-field and vibronic transitions of the $^2F_{5/2} \rightarrow {}^2F_{7/2}$ optical multiplet. Trace amounts of Er^{3+} and Tm^{3+} are also present in the 10%Yb^{3+}:LLF crystals as evident from the following PL transitions: $^1G_4 \rightarrow {}^3H_6$ (Tm^{3+}, 450–500 nm), $^2H_{11/2} \rightarrow {}^4I_{15/2}$ (Er^{3+}, 515–525 nm), $^4S_{3/2} \rightarrow {}^4I_{15/2}$, $^2H_{9/2} \rightarrow {}^4I_{13/2}$ (Er^{3+}, 545–555 nm), $^4F_{9/2} \rightarrow {}^4I_{15/2}$ (Er^{3+}, 620–680 nm), $^3H_4 \rightarrow {}^3H_6$ (Tm^{3+}, 750–840 nm) (Figure S5, Supporting Information).

To evaluate whether 10%Yb^{3+}:LLF could refrigerate silicon-nitride TEM windows, individual LLF grains were transferred to TEM windows using a nanomanipulator and optically excited in vacuum at different irradiances from 0.03 to 0.85 MW cm^{-2} as shown in **Figure 3**. Temperature calibration spectra of individual LLF grains were collected in an optical cryostat at temperatures from 170 K to 295 K using low laser irradiance (0.03 MW cm^{-2}) to minimize photothermal effects from optical excitation. The mean wavelengths of the spectra can be obtained by calculating the "spectral centroid" representing the first moment $\lambda_f = \frac{\sum I(\lambda_i)}{\sum I(\lambda_i)/\lambda_i}$.[58] Here, the entire spectral window is integrated. As the temperature of LLF grains increases, the mean wavelength blueshifts due to the changing excited-state Boltzman population distribution, which redistributes intensities across the various peaks of the spectrum (Figures 2c and Figure 3d). Changes in the mean wavelength are directly correlated to a change in the crystal temperature. As shown in Figure 3e, this dependence can be expressed as $\lambda = -0.05 \cdot T + 984.49$ where λ is the mean wavelength and T is the Yb^{3+}:LLF crystal temperature. The decrease (increase) in the mean wavelength with increasing irradiance reflects an increase (decrease) in the internal lattice temperature when supported on the in situ TEM window (Figure 3; Figure S7, Supporting Information). According to Figure S7d in

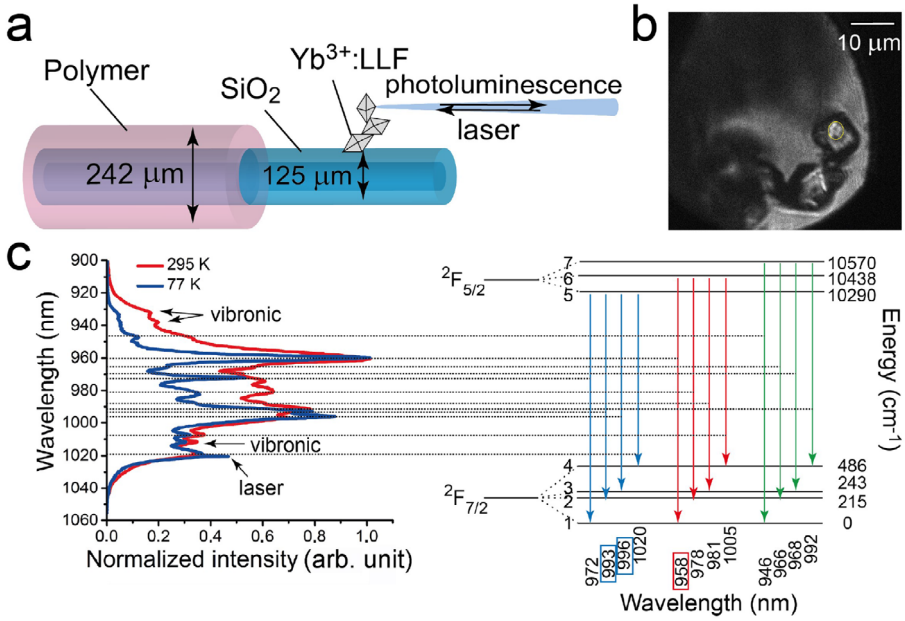

Figure 2. a) Schematic of 10%Yb^{3+}:LLF microcrystals on a SiO_2 optical fiber in vacuum; b) Optical micrograph of 10%Yb^{3+}:LLF microcrystals on a SiO_2 optical fiber; c) Assignment of the crystal-field transitions of Yb^{3+} in LLF following excitation with a pulsed laser at $\lambda = 1020$ nm.

the Supporting Information, saturation is visible at high laser irradiances. However, no other nonlinear effects such as lasing are observed. Therefore, the PL measured at high irradiance still comes from a thermalized excited-state population of Yb^{3+} ions, and its intensity distribution reflects the internal lattice temperature. At room temperature, the PL spectrum has a mean wavelength of 970.05 nm. At a laser irradiance of 0.854 MW cm^{-2}, the mean wavelength shifts to 971.04 nm from which the temperature can be estimated as 20.4 K below room temperature (Figure 3f). This result demonstrates successful net cooling of an individual Yb^{3+}:LLF crystallite adhered to a Si_3N_4 TEM window, and shows that these excitation conditions do not cause net heating of the sample by, for example, excessive laser absorption by the underlying Si_3N_4 layer.

Direct measurement of the Si_3N_4 TEM window temperature using non-contact optical thermometry is complicated by weak background Si_3N_4 fluorescence (Figure S11, Supporting Information). To test for cooling across the LLF/Si_3N_4 interface, we instead measured the internal temperatures of Si_3N_4 photonic waveguides with appended laser-cooled Yb^{3+}:LLF microcrystals, using the thermooptic coefficient (dn/dT) of Si_3N_4 as our temperature probe. For this measurement, a waveguide-coupled Si_3N_4 nanobeam cavity was fabricated,[61,62] to which a Yb^{3+}:LLF crystal was attached. The transmitted cavity eigenmodes were then monitored as a function of Yb^{3+}:LLF microcrystal irradiation. Details for the fabrication and measurement of the Si_3N_4 cavity are provided in the supporting information (Figure S12, Supporting Information). The internal temperature of the Si_3N_4 cavity was found to decrease by 1.8 ± 1.2 K upon increasing 1020 nm excitation to 0.482 MW cm^{-2}, despite the presence of a thick underlying silicon substrate that is susceptible to heating from the transmitted 1020 nm laser beam (Figure S13, Supporting Information). These data demonstrate that Si_3N_4 can be cooled by laser cooling an adjacent Yb^{3+}:LLF microcrystal, and we infer from this result that the Si_3N_4 TEM window in Figure 3 is also cooled when its appended Yb^{3+}:LLF microcrystal is irradiated. The TEM window is observed to cool more than the waveguide due the lack of the underlying silicon substrate. Analogous laser cooling trends were observed for 10%Yb^{3+}:LLF grains on an optical fiber in vacuum (Figure S8, Supporting Information) and in air (Figure S9, Supporting Information) and also for individual 10%Yb^{3+}:LLF grains optically trapped in water (Figure S10, Supporting Information). Yb^{3+}:YLF has also been shown recently to refrigerate a semiconducting cantilever device.[59][60]

Using the laser cooling data in Figure 3f, we performed finite-element simulations of the steady state temperatures across the Si_3N_4 TEM window during laser cooling of the Yb^{3+}:LLF microcrystal in that experiment. Assuming the bottom surface of the silicon substrate is maintained at room temperature (298 K) and the temperature of the Yb^{3+}:LLF microscrystal is 277 K, as measured by its luminescence, finite element calculations indicate that the majority of the 200 micrometer long Si_3N_4 window remains below ≈283 K, reaching a base temperature of ≈279.4 K directly below the Yb^{3+}:LLF microcrystal (Figure 3c; Figure S14, Supporting Information). These results support the experimental conclusion that it is possible to laser refrigerate Yb^{3+}:LLF crystallites supported on a TEM window without direct laser heating of the window or its support, demonstrating laser cooling as a viable approach for contactless refrigeration of in situ and cryo-TEM experiments.

3. Conclusion

We report the first experimental demonstration of solid-state laser refrigeration of electron-transparent, in situ TEM windows. 10%Yb^{3+}:LLF microcrystals were grown using a low-cost, scalable hydrothermal process. Individual 10%Yb^{3+}:LLF microcrystals were transferred to electron-transparent Si_3N_4 windows and

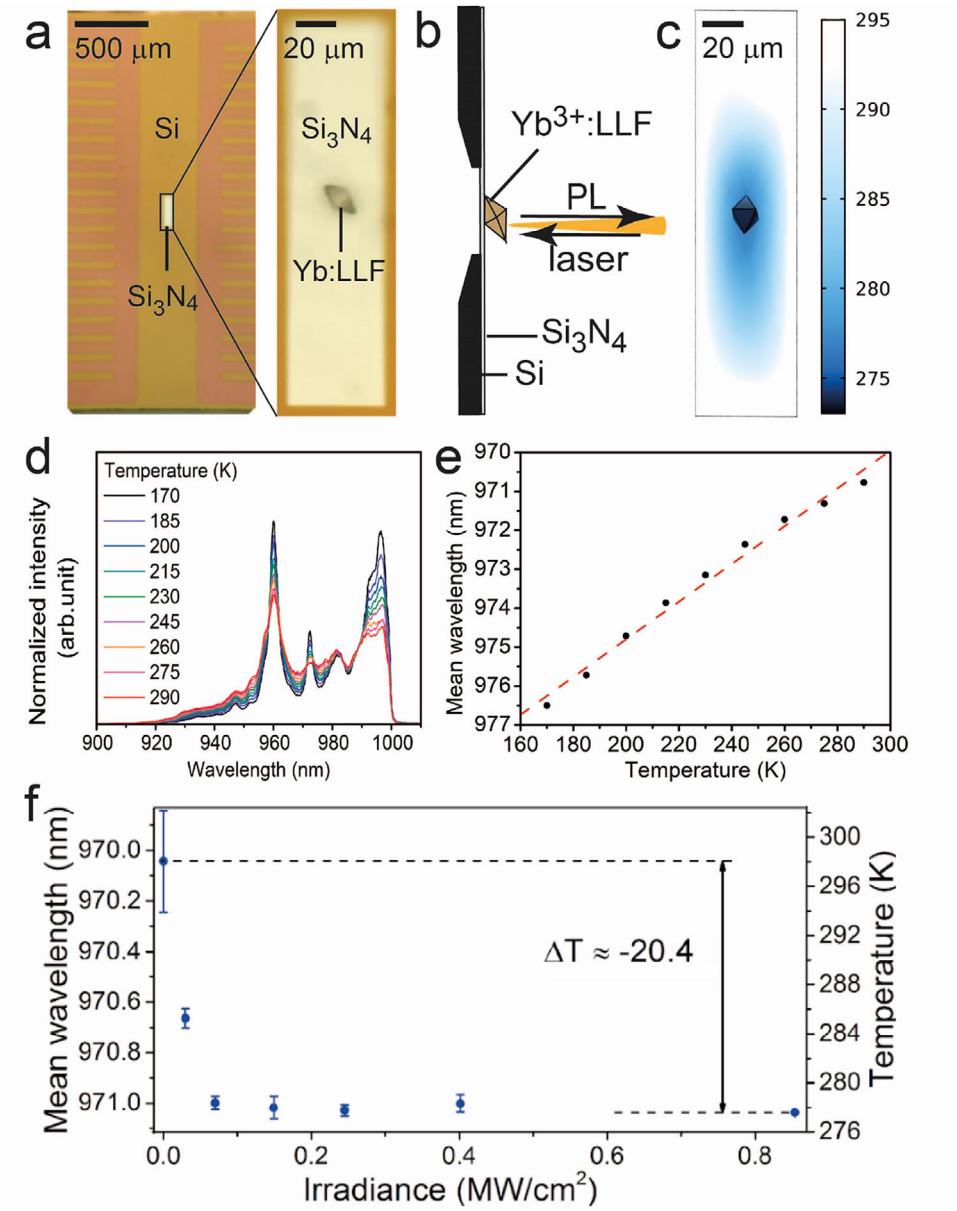

Figure 3. a) Photograph of a Si_3N_4 TEM window. Inset: micrograph of a 10%Yb^{3+}:LLF microcrystal on a Si_3N_4 TEM window; b) Schematic of 10%Yb^{3+}:LLF microcrystals on a Si_3N_4 TEM window in vacuum; c) Finite-element simulation of the steady-state temperature around the laser-cooled LLF microcrystal on the Si_3N_4 window; d) Temperature-dependent PL of a 10%Yb^{3+}:LLF microcrystal on a Si_3N_4 TEM window in vacuum. The spectra are normalized by area; e) The calibrated mean wavelength (λ)–temperature (T) dependence expressed as $\lambda = -0.05 \cdot T + 984.49$; f) The mean wavelength – laser irradiance dependence measured for 10%Yb^{3+}:LLF on a Si_3N_4 TEM window in vacuum.

irradiated using a near-infrared laser. Analysis of the Yb^{3+} luminescence spectrum revealed laser cooling in vacuum (10^{-3} torr) by more than 20.4 K below room temperature at an irradiance of 0.854 MW cm^{-2}, and modeling indicates bulk cooling of the Si_3N_4 window by ≈15 K at steady state, despite the nearby room-temperature silicon substrate. Contact cooling across the LLF/Si_3N_4 interface was independently verified by demonstrating laser cooling of a Si_3N_4 photonic waveguide. These results suggest a new all-optical approach for controlling temperatures during in situ and cryo-TEM measurements.

4. Experimental Section

Lutetium nitrate ($Lu(NO_3)_3$, 99.999% purity) and ytterbium nitrate ($Yb(NO_3)_3$, 99.99% purity) were used for hydrothermal synthesis of Yb^{3+}:LLF as purchased from Sigma-Aldrich. The RE nitrates were dissolved in Millipore deionized (DI) water to achieve a stock concentration (0.5 M) of the respective nitrate. Ethylenediaminetetraacetic acid (EDTA, 99% purity, Sigma-Aldrich), lithium hydroxide (LiOH, 99.995% purity, Sigma-Aldrich), lithium fluoride (LiF, 99.98% purity, Sigma-Aldrich), and ammonium difluoride (NH_4HF_2, 99% purity, Sigma-Aldrich) were analytical grade and were used directly in the synthesis without any purification. For this synthesis, 7.2 mL of 0.5 M $Lu(NO_3)_3$ and 0.8 mL of 0.5 M

$Yb(NO_3)_3$ were mixed with 1.17 g of EDTA and 0.45 g of LiOH in 1 mL Millipore DI water at 80 °C while stirring for 1 h to form solution A. Subsequently, 0.21 g of LiF and 0.68 g of NH_4HF_2 were dissolved in 7 mL Millipore DI water at 70 °C while stirring for 1 h to form solution B. Solutions A and B were mixed together while stirring for 20 min to form a homogeneous white suspension, which was transferred to a 23-mL Teflon-lined autoclave and heated to 220 °C for 72 h. After the autoclave cooled to room temperature, the 10%Yb^{3+}:LLF particles were recovered by centrifuging and washing with ethanol and Millipore DI water three times. The final white powder was obtained by calcining at 300 °C for 2 h in air.

PL spectra were registered using a home-built micro-PL setup. A 50x long working distance (17 mm) objective (Nikon) was used to focus the laser on the samples to a focal spot of radius 1.15 µm. Spectral data were acquired using a 1020 nm diode laser (Qphotonics) with 1000 nm short-pass filter before the spectrometer. PL spectra from Yb^{3+}-doped LLF host crystals were collected using a liquid-nitrogen-cooled Si detector in an Acton SpectraPro 500i spectrograph (Princeton Instruments). The mean wavelength–temperature calibration was performed using a Janis ST500 optical cryostat and Lake Shore 335 temperature controller with resolution 0.01 K.

Supporting Information

Supporting Information is available from the Wiley Online Library or from the author.

Acknowledgements

E.D., M.D., D.G., A.M., and P.P. acknowledge support from the National Science Foundation through the UW Molecular Engineering Materials Center, a Materials Research Science and Engineering Center (DMR-1719797). A.P., X.X., and P.P. acknowledge financial support from the MURI:MARBLe project under the auspices of the Air Force Office of Scientific Research (Award No. FA9550-16-1-0362). Part of this work was conducted at the Molecular Analysis Facility, a National Nanotechnology Coordinated Infrastructure site at the University of Washington, which is supported in part by the National Science Foundation (grant ECC-1542101). K.B. and A.M. acknowledge support from the Russian Foundation for Basic Research (Grant No. 18-32-20142).

Conflict of Interest

The authors declare no conflict of interest.

Author Contributions

E.D. performed materials synthesis and characterization, data acquisition, data analysis, and both writing and figure preparation. X.X. contributed materials synthesis and characterization. M.L. contributed electron microscopy characterization data. A.P., M.D., and D.G. contributed low-temperature PL spectra. A.P. contributed sample preparation, data processing scripts with the heat transfer simulation. X.X. and A.P. contributed equally to this work. K.B., A.D.M., and M.P. contributed temperature-dependent phonon spectra, N.N. and S.K. contributed room-temperature phonon spectra of LLF materials. Y.C. and A.M. contributed to the fabrication and characterization of silicon nitride nanobeam cavity. P.P. conceived of and directed experiments, participated in data interpretation, figure design, and the writing of the final manuscript. All coauthors proofread the final manuscript.

Data Availability Statement

The data that support the findings of this study are available from the corresponding author upon reasonable request.

Keywords

anti-Stokes photoluminescence, hydrothermal synthesis, in situ TEM, laser cooling, silicon nitride

Received: January 15, 2021
Revised: June 4, 2021
Published online: August 16, 2021

[1] K. H. Nagamanasa, H. Wang, S. Granick, *Adv. Mater.* **2017**, *29*, 1703555.
[2] N. Wang, Q. Sun, J. Yu, *Adv. Mater.* **2019**, *31*, 1803966.
[3] M. Textor, N. de Jonge, *Nano Lett.* **2018**, *18*, 3313.
[4] S. M. Rehn, M. R. Jones, *ACS Energy Lett.* **2018**, *3*, 1269.
[5] B. H. Kim, J. Yang, D. Lee, B. K. Choi, T. Hyeon, J. Park, *Adv. Mater.* **2018**, *30*, 1703316.
[6] K. He, A. Nie, Y. Yuan, S. M. Ghodsi, B. Song, E. Firlar, J. Lu, Y.-p. Lu, T. Shokuhfar, C. M. Megaridis, R. Shahbazian-Yassar, *ACS Appl. Nano Mater.* **2018**, *1*, 5430.
[7] Y. Yuan, K. Amine, J. Lu, R. Shahbazian-Yassar, *Nat. Commun.* **2017**, *8*, 15806.
[8] C. Yang, J. Han, P. Liu, C. Hou, G. Huang, T. Fujita, A. Hirata, M. Chen, *Adv. Mater.* **2017**, *29*, 1702752.
[9] J. Vance, S. Dillon, *Chem. Commun.* **2017**, *53*, 4930.
[10] M. L. Tate, D. A. Blom, M. Avdeev, H. E. A. Brand, G. J. McIntyre, T. Vogt, I. R. Evans, *Adv. Funct. Mater.* **2017**, *27*, 1605625.
[11] S.-Y. Lee, L. Wu, A. S. Poyraz, J. Huang, A. C. Marschilok, K. J. Takeuchi, E. S. Takeuchi, M. Kim, Y. Zhu, *Adv. Mater.* **2017**, *29*, 1703186.
[12] J. Wu, H. Shan, W. Chen, X. Gu, P. Tao, C. Song, W. Shang, T. Deng, *Adv. Mater.* **2016**, *28*, 9686.
[13] C. Ophus, J. Ciston, J. Pierce, T. R. Harvey, J. Chess, B. J. McMorran, C. Czarnik, H. H. Rose, P. Ercius, *Nat. Commun.* **2016**, *7*, 10719.
[14] K. He, S. Zhang, J. Li, X. Yu, Q. Meng, Y. Zhu, E. Hu, K. Sun, H. Yun, X.-Q. Yang, Y. Zhu, H. Gan, Y. Mo, E. A. Stach, C. B. Murray, D. Su, *Nat. Commun.* **2016**, *7*, 11441.
[15] J. R. Jokisaari, J. A. Hachtel, X. Hu, A. Mukherjee, C. Wang, A. Konecna, T. C. Lovejoy, N. Dellby, J. Aizpurua, O. L. Krivanek, J.-C. Idrobo, R. F. Klie, *Adv. Mater.* **2018**, *30*, 1802702.
[16] G. Zhu, M. L. Sushko, J. S. Loring, B. A. Legg, M. Song, J. A. Soltis, X. Huang, K. M. Rosso, J. J. De Yoreo, *Nature* **2021**, *590*, 416.
[17] Q. Cheek, E. Fahrenkrug, S. Hlynchuk, D. H. Alsem, N. J. Salmon, S. Maldonado, *ACS Nano* **2020**, *14*, 2869.
[18] D. J. Banner, E. Firlar, P. Rehak, A. H. Phakatkar, T. Foroozan, J. K. Osborn, L. V. Sorokina, S. Narayanan, T. Tahseen, Y. Baggia, P. Král, T. Shokuhfar, R. Shahbazian-Yassar, *Adv. Funct. Mater.* **2021**, *31*, 2007736.
[19] A. E. S. Van Driessche, N. Van Gerven, P. H. H. Bomans, R. R. M. Joosten, H. Friedrich, D. Gil-Carton, N. A. J. M. Sommerdijk, M. Sleutel, *Nature* **2018**, *556*, 89.
[20] M. Reifarth, S. Hoeppener, U. S. Schubert, *Adv. Mater.* **2018**, *30*, 1703704.
[21] M. Piffoux, N. Ahmad, J. Nelayah, C. Wilhelm, A. Silva, F. Gazeau, D. Alloyeau, *Nanoscale* **2018**, *10*, 1234.
[22] M. Elbaum, *Adv. Mater.* **2018**, *30*, 1706681.
[23] A. Arnould, F. Caputo, M. Bacia, I. Texier, M. Escude, D. Boutry, A. Auger, R. Soulas, J.-F. Damlencourt, *Microsc. Microanal.* **2018**, *24*, 314.
[24] Y. Li, Y. Li, A. Pei, K. Yan, Y. Sun, C.-L. Wu, L.-M. Joubert, R. Chin, A. L. Koh, Y. Yu, *Science* **2017**, *358*, 506.
[25] J. J. De Yoreo, N. A. Sommerdijk, *Nat. Rev. Mater.* **2016**, *1*, 16035.
[26] A. B. Yankovich, B. Berkels, W. Dahmen, P. Binev, S. I. Sanchez, S. A. Bradley, A. Li, I. Szlufarska, P. M. Voyles, *Nat. Commun.* **2014**, *5*, 4155.
[27] A. Matatyaho Ya'akobi, Y. Talmon, *Acc. Chem. Res.* **2021**, *54*, 2100.

[28] D. A. M. De Winter, C. Hsieh, M. Marko, M. F. Hayles, *J. Microsc.* **2021**, *281*, 125.
[29] Y. Zhu, Z. Gui, Q. Wang, F. Meng, S. Feng, B. Han, P. Wang, L. Huang, H.-L. Wang, M. Gu, *Nano Energy* **2020**, *73*, 104820.
[30] D. V. Seletskiy, S. D. Melgaard, S. Bigotta, A. Di Lieto, M. Tonelli, M. Sheik-Bahae, *Nat. Photonics* **2010**, *4*, 161.
[31] S. D. Melgaard, D. V. Seletskiy, A. Di Lieto, M. Tonelli, M. Sheik-Bahae, *Opt. Lett.* **2013**, *38*, 1588.
[32] S. D. Melgaard, A. R. Albrecht, M. P. Hehlen, M. Sheik-Bahae, *Sci. Rep.* **2016**, *6*, 20380.
[33] P. B. Roder, B. E. Smith, X. Zhou, M. J. Crane, P. J. Pauzauskie, *Proc. Natl. Acad. Sci. USA* **2015**, *112*, 15024.
[34] X. Zhou, B. E. Smith, P. B. Roder, P. J. Pauzauskie, *Adv. Mater.* **2016**, *28*, 8658.
[35] P. Pringsheim, *Z. Phys.* **1929**, *57*, 739.
[36] X. Xia, A. Pant, A. S. Ganas, F. Jelezko, P. J. Pauzauskie, *Adv. Mater.* **2020**, *32*, 1905406.
[37] S. Yatsiv, *Adv. Quantum Electron.* **1961**, *200*.
[38] T. Kushida, J. Geusic, *Phys. Rev. Lett.* **1968**, *21*, 1172.
[39] R. I. Epstein, M. I. Buchwald, B. C. Edwards, T. R. Gosnell, C. E. Mungan, *Nature* **1995**, *377*, 500.
[40] E. S. de Lima Filho, G. Nemova, S. Loranger, R. Kashyap, *Opt. Express* **2013**, *21*, 24711.
[41] R. Remski, L. James, K. Gooen, B. Bartolo, A. Linz, *IEEE J. Quantum Electron.* **1969**, *5*, 214.
[42] J. R. Thornton, W. D. Fountain, G. W. Flint, T. G. Crow, *Appl. Opt.* **1969**, *8*, 1087.
[43] N. Agladze, M. Popova, *Solid State Commun.* **1985**, *55*, 1097.
[44] N. Agladze, M. Popova, G. Zhizhin, V. Egorov, M. Petrova, *Phys. Rev. Lett.* **1991**, *66*, 477.
[45] M. Brown, K. Roots, W. Shand, *J. Phys. C: Solid State Phys.* **1969**, *2*, 593.
[46] S. Miller, H. Rast, H. Caspers, *J. Chem. Phys.* **1970**, *52*, 4172.
[47] J. Miller, E. Sharp, *J. Appl. Phys.* **1970**, *41*, 4718.
[48] R. Watts, *J. Chem. Phys.* **1970**, *53*, 3552.
[49] D. Gabbe, A. Harmer, *J. Cryst. Growth* **1968**, *3*, 544.
[50] A. T. M. A. Rahman, P. F. Barker, *Nat. Photonics* **2017**, *11*, 634.
[51] A. Sen, S. Chaplot, R. Mittal, *Phys. Rev. B* **2001**, *64*, 024304.
[52] B. Zhong, J. Yin, Y. Jia, L. Chen, Y. Hang, J. Yin, *Opt. Lett.* **2014**, *39*, 2747.
[53] B. Zhong, H. Luo, Y. Shi, J. Yin, *Opt. Eng.* **2016**, *56*, 011102.
[54] B. Zhong, H. Luo, L. Chen, Y. Shi, J. Yin, *SPIE OPTO* **2016**, *9765*, 6.
[55] B. Zhong, H. Luo, Y. Lei, Y. Shi, J. Yin, *SPIE Defense + Security* **2017**, *10180*, 7.
[56] A. Volpi, G. Cittadino, A. Di Lieto, A. Cassanho, H. P. Jenssen, M. Tonelli, *Opt. Eng.* **2016**, *56*, 011105.
[57] S. Salaün, M. Fornoni, A. Bulou, M. Rousseau, P. Simon, J. Gesland, *J. Phys.: Condens. Matter* **1997**, *9*, 6941.
[58] D. V. Seletskiy, S. D. Melgaard, R. I. Epstein, A. Di Lieto, M. Tonelli, M. Sheik-Bahae, *J. Lumin.* **2013**, *133*, 5.
[59] A. Pant, B. E. Smith, M. J. Crane, X. Zhou, M. B. Lim, S. A. Frazier, E. J. Davis, P. J. Pauzauskie, *J. Phys. Chem. C* **2018**, *122*, 7525.
[60] A. Pant, X. Xia, E. J. Davis, P. J. Pauzauskie, *Nat. Commun.* **2020**, *11*, 3235.
[61] T. K. Fryett, Y. Chen, J. Whitehead, Z. M. Peycke, X. Xu, A. Majumdar, *ACS Photonics* **2018**, *5*, 2176.
[62] Y. Chen, A. Ryou, M. R. Friedfeld, T. Fryett, J. Whitehead, B. M. Cossairt, A. Majumdar, *Nano Lett.* **2018**, *18*, 6404.